Glaucoma

In Vivo 3-Dimensional Strain Mapping Confirms Large Optic Nerve Head Deformations Following Horizontal Eye Movements

Xiaofei Wang,[1] Meghna R. Beotra,[1] Tin Aung Tun,[1,2] Mani Baskaran,[2,3] Shamira Perera,[2,3] Tin Aung,[2–4] Nicholas G. Strouthidis,[2,5,6] Dan Milea,[2,3] and Michaël J. A. Girard[1,2]

[1]Ophthalmic Engineering & Innovation Laboratory, Department of Biomedical Engineering, Faculty of Engineering, National University of Singapore, Singapore
[2]Singapore Eye Research Institute, Singapore National Eye Centre, Singapore
[3]Duke-NUS, Singapore
[4]Department of Ophthalmology, Yong Loo Lin School of Medicine, National University of Singapore, Singapore
[5]NIHR Biomedical Research Centre, Moorfields Eye Hospital NHS Foundation Trust and UCL Institute of Ophthalmology, London, United Kingdom
[6]Discipline of Clinical Ophthalmology and Eye Health, University of Sydney, Sydney, New South Wales, Australia

Purpose. To measure lamina cribrosa (LC) strains (deformations) following abduction and adduction in healthy subjects and to compare them with those resulting from a relatively high acute intraocular pressure (IOP) elevation.

Methods. A total of 16 eyes from 8 healthy subjects were included. Among the 16 eyes, 11 had peripapillary atrophy (PPA). For each subject, both optic nerve heads (ONHs) were imaged using optical coherence tomography (OCT) at baseline (twice), in different gaze positions (adduction and abduction of 20°) and following an acute IOP elevation of approximately 20 mm Hg from baseline (via ophthalmodynamometry). Strains of LC for all loading scenarios were mapped using a three-dimensional tracking algorithm.

Results. In all 16 eyes, LC strains induced by adduction and abduction were 5.83% ± 3.78% and 3.93% ± 2.57%, respectively, and both significantly higher than the control strains measured from the repeated baseline acquisitions ($P < 0.01$). Strains of LC in adduction were on average higher than those in abduction, but the difference was not statistically significant ($P = 0.07$). Strains of LC induced by IOP elevations (on average 21.13 ± 7.61 mm Hg) were 6.41% ± 3.21% and significantly higher than the control strains ($P < 0.0005$). Gaze-induced LC strains in the PPA group were on average larger than those in the non-PPA group; however, the relationship was not statistically significant.

Conclusions. Our results confirm that horizontal eye movements generate significant ONH strains, which is consistent with our previous estimations using finite element analysis. Further studies are needed to explore a possible link between ONH strains induced by eye movements and axonal loss in optic neuropathies.

Keywords: eye movements, glaucoma, optic nerve head, lamina cribrosa, optical coherence tomography

Glaucoma is characterized by an irreversible damage of retinal ganglion cells within the optic nerve head (ONH). We also know that elevated intraocular pressure (IOP) is associated with increased prevalence[1] and incidence[2] of glaucoma. However, some patients with elevated IOP never develop glaucoma—a condition referred to as ocular hypertension. Furthermore, glaucoma occurs nearly as often in patients with either normal IOP levels (normal tension glaucoma) or elevated IOP levels (high tension glaucoma), and does so without distinct etiology.[3] In brief, our current understanding of glaucoma is insufficient: we know that IOP is a main, albeit not the only predisposing risk factor in the development and progression of this pathology.[4]

The "standard" biomechanical theory of glaucoma hypothesizes that elevated (or fluctuating) IOP deforms the ONH tissues, including the lamina cribrosa (LC), and that these deformations drive retinal ganglion cell injury and death.[5] Deformations (or strains) of ONH, rather than IOP, may have the potential to be used for monitoring glaucoma development and progression. Interestingly, IOP is not the only load that can induce ONH deformations in vivo. Chronically elevated cerebrospinal fluid pressure (CSFP) has been shown to significantly deform the ONH, resulting in anterior deformations and bending of ONH connective tissues (LC and peripapillary sclera), which causes loss of vision that is associated with "swelling" of ONH tissues.[6] Recently, we have theorized about a third loading mechanism that could significantly deform the ONH. Specifically, using magnetic resonance imaging (MRI) and finite element modeling, we have demonstrated that eye movements (in both adduction and

abduction) could generate large deformations within the ONH through the pulling action of the optic nerve (ON) sheaths.[7] Such deformations were considered significant as they were predicted to be as high as those induced by an IOP of 50 mm Hg. Another independent MRI study of eye movements also confirmed that this scenario could be plausible through the presence of a taut ON in adduction.[8] However, to date, because of the low resolution of MRI, ONH deformations could only be predicted using finite element modeling rather than directly measured experimentally in subjects.

The aim of this study was to measure for the first time LC mechanical strains (the engineering definition of deformation) in both adduction and abduction in healthy subjects, using optical coherence tomography (OCT) and recently described three-dimensional (3D) strain mapping technology.[9,10] We further aimed to compare the magnitude of those strains with those resulting from a high acute IOP elevation to approximately 35 to 40 mm Hg.

METHODS

We combined OCT imaging with a 3D strain mapping algorithm to extract the 3D deformations of the LC at different gaze positions (in both adduction and abduction) and following acute elevations of IOP. Below is a detailed description of our OCT and 3D strain mapping protocols.

Subjects

For this study, 10 healthy subjects were recruited at the Singapore Eye Research Institute. These subjects were not attending the hospital eye service for any clinical reason and had no other relevant pathology. Because the aim of this study was to explore how eye movements could deform the ONH, we did not exclude subjects with high myopia. However, two subjects were excluded from the analysis because of the poor visibility of the LC in the acquired OCT volumes as graded manually (XW). Among the remaining 16 eyes, 11 of them had peripapillary atrophy (PPA), as defined by the presence of either peripapillary beta or gamma zone from scanning laser ophthalmoscopy images and OCT volumes (manually graded; TAT, XW).[11]

Each subject underwent the following ocular examinations for both eyes: (1) measurement of refraction using an autokeratometer (RK-5; Canon, Tokyo, Japan); (2) measurement of axial length, central corneal thickness (CCT) and anterior chamber depth (ACD) using a commercial device (Lenstar LS 900; Haag-Streit AG, Switzerland); (3) measurement of IOP using an applanation tonometer (Tonopen AVIA; Reichert, Inc., Depew, NY, USA) before and after IOP elevation; (4) imaging of the ONH using OCT as described in details below.

Demographics and clinical data for all included subjects are listed in Table 1. The protocol was approved by the SingHealth Centralized Institutional Review Board and adhered to the tenets of the Declaration of Helsinki. Written voluntary informed consent was obtained from each subject.

OCT Imaging

Each eye's ONH was imaged five times with spectral-domain OCT (Spectralis; Heidelberg Engineering GmbH, Heidelberg, Germany). Each set of images (raster scan) comprised 97 serial horizontal B-scans (each composed of 384 A-scans) covering a rectangular region of $15° \times 10°$ centered on the ONH. The distance between consecutive B-scans was slightly different across eyes and was on average 33.4 ± 1.9 μm. Similarly, the

TABLE 1. Demographic and Ophthalmic Characteristics of the Study Subjects

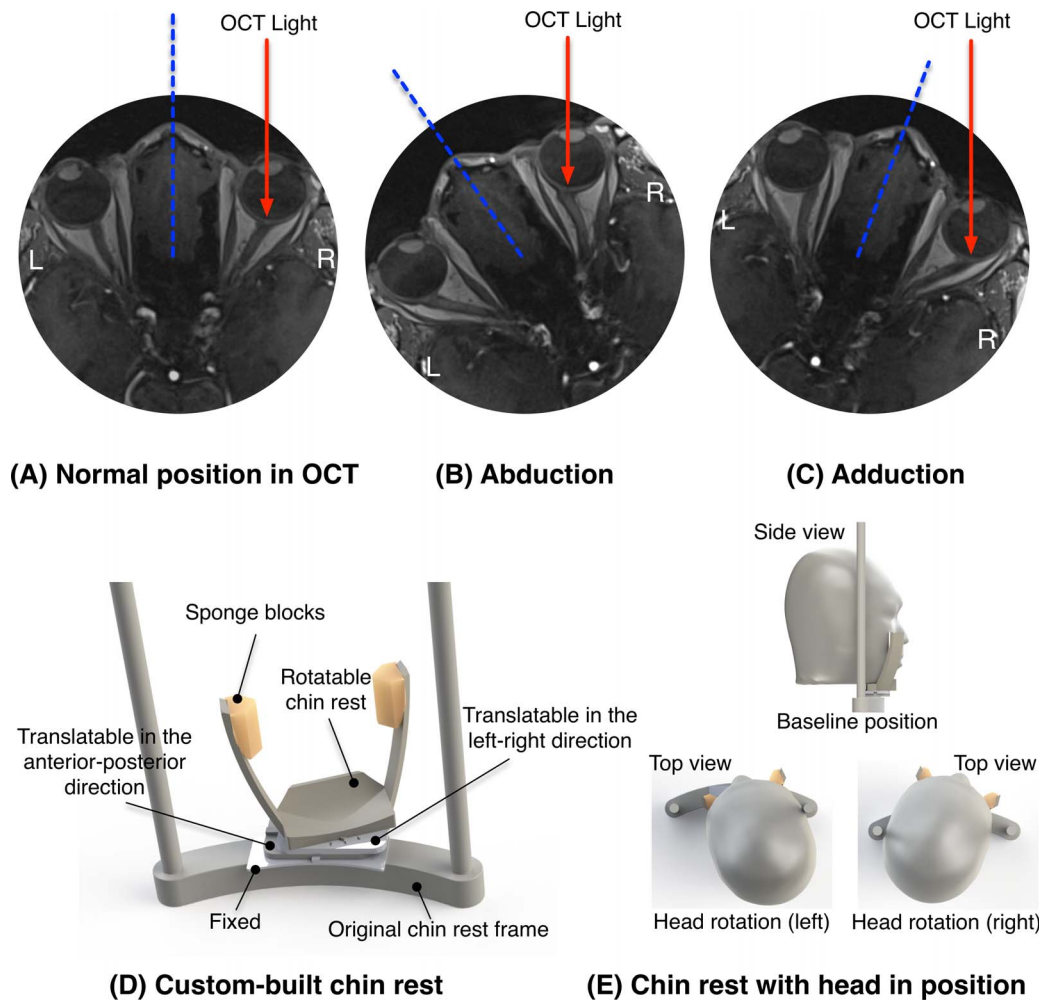| Parameters	Mean ± SD	Range
Age, y	25 ± 3	21–29
Sex, F/M	2/6	NA
Ethnicity	1 Indian; 2 Vietnamese; 5 Chinese	NA
Axial length, mm	25.11 ± 1.26	23.85–27.77
CCT, μm	562 ± 25	531–600
ACD, mm	3.60 ± 0.25	3.33–4.17
Lens thickness, mm	3.57 ± 0.19	3.28–3.84
Refractive error, diopters	–3.73 ± 2.93	–0.5 to –10.75
Baseline IOP, mm Hg	18.06 ± 2.57	14 – 21

NA, not applicable.

lateral resolution of each B-scan varied slightly across eyes, and was on average 12.5 ± 0.7 μm horizontally and 3.9 ± 0.0 μm axially. Each B-scan was averaged 20 times during acquisition to reduce speckle noise.

OCT Imaging With Unaltered IOP and Gaze Position (Control). For each eye, two OCT volumes of the ONH were acquired repeatedly for each eye in the baseline OCT position (as defined below) without IOP elevation and without changes in gaze position. The first OCT volume was considered the baseline (reference) volume, from which all strain calculations were computed. The second OCT volume was referred to as the "repeated" volume. To ensure that LC deformations are indeed present following a change in IOP or in gaze position, they need to be significantly higher than the control deformations observed between the baseline and repeated volumes.

It should also be noted that standard OCT acquisitions of the ONH are not performed in the primary gaze position. This is because the pupil and the ONH need to be aligned with the OCT objective, requiring subjects to slightly gaze left with their right eye, or gaze right with their left eye (Fig. 1A). Therefore, in this paper, we used the terminology "baseline gaze position" to refer to the eye position during a standard OCT scan. The amplitudes of eye rotations reported in this study were all relative to this baseline gaze position.

OCT Imaging Following Changes in Gaze Position. Two additional OCT volumes were acquired at different gaze positions for each eye: one with the eye in nasal gaze (adduction; 20°) and one with the eye in temporal gaze (abduction; 20°), respectively. Intraocular pressure was not altered in these two scans. Eye rotation was achieved by rotating the subject's head while keeping the eye aligned with the fixed OCT objective (Figs. 1B, 1C). The subject's head was fixed on a custom-built 3D-printed chin rest, which is rotatable and translatable. This chin rest allowed precise control of the head rotation magnitude to make sure that the eye rotation angles were accurately achieved.

OCT Imaging With Acute Changes in IOP. One additional OCT volume was acquired in the baseline gaze position with IOP transiently increased to around 40 mm Hg using a custom-made ophthalmodynamometer (spring-loaded indenter) as in our previous study.[12] Briefly, the ophthalmodynamometer was held perpendicular to the anterior sclera and gently applied an external force through the temporal side of the lower eyelid. The constant applied force was 0.64 N (82.5 g) as calibrated using a uniaxial tensile tester (Instron-5848; Instron, Inc., Noorwood, MA, USA). This force level was chosen based on our preliminary data obtained from 20 healthy eyes in order to achieve an IOP increase of approximately 20 mm Hg from baseline. After IOP elevation,

(A) Normal position in OCT   (B) Abduction   (C) Adduction

(D) Custom-built chin rest   (E) Chin rest with head in position

FIGURE 1. (**A**) Standard OCT acquisition in "baseline eye position" illustrated using an MRI image of a healthy subject. (**B**) Acquisition of OCT in abduction after a counterclockwise head rotation of 20° from the baseline head position in (**A**). (**C**) Acquisition of OCT in adduction after a clockwise head rotation of 20° from the baseline head position in (**A**). Note that head rotations in these MRI images were larger than 20° and were used for illustration purpose only. L, left; R, right. (**D**) Schematic of our custom-built chin rest integrated to the OCT device. (**E**) Chin rest with the subject's head in three different positions (baseline, head rotation to the left for imaging a right eye in abduction as in (**B**), head rotation to the right for imaging a right eye in adduction as in (**C**).

IOP was held constant and remeasured with a Tonopen (Reichert, Inc.) while the indenter was maintained in place. The measured mean IOP increase for all eyes was 21.13 ± 7.61 mm Hg.

Image Enhancement With Adaptive Compensation

To improve LC visibility, raw OCT images were enhanced using adaptive compensation. Adaptive compensation is an OCT postprocessing technique that removes blood vessel shadows and enhances tissue contrast. It has been shown to significantly improve the visibility of the anterior LC, its insertions, and other ocular structures.[13,14]

Digital Reconstruction of the LC

Each compensated baseline OCT volume was manually segmented using 3D software (Amira, version 5.6; FEI, Hillsboro, OR, USA) to digitally reconstruct the LC. Note that only parts of the LC that were visible from the compensated OCT volume were segmented. In most cases, full-thickness segmentation of the LC could not be achieved because of poor or absent visibility of the posterior LC boundary.

In Vivo 3D Displacement/Strain Mapping of the LC Following Changes in Gaze Position and in IOP

For each eye, we acquired four sets of OCT volumes, each set comprising two OCT volumes (set 1: baseline + repeated volume with unaltered IOP and gaze position [control]; set 2: baseline + adduction volume; set 3: baseline + abduction volume; set 4: baseline + acute IOP elevation volume). For each set, the second OCT volume was first reoriented to align with the baseline volume through rigid translation/rotation transformations using 3D software (Amira, version 5.6; FEI). This rigid registration was performed using a voxel-based algorithm that maximized mutual information between two volumes.[15] We then used a 3D tracking algorithm designed to extract local 3D tissue displacements between two OCT volumes captured under different loading scenarios (as proposed herein). This algorithm was found to be robust to OCT speckle noise—the noise inherent to OCT—and was used recently to map local 3D strains (deformations) of subjects' ONHs following a change in IOP in vivo via trabeculectomy.[10] More technical details of our 3D tracking algorithm can be found in our previous publications.[9,10] For each set of two OCT volumes, we computed LC displacements at the nodes of the digitally
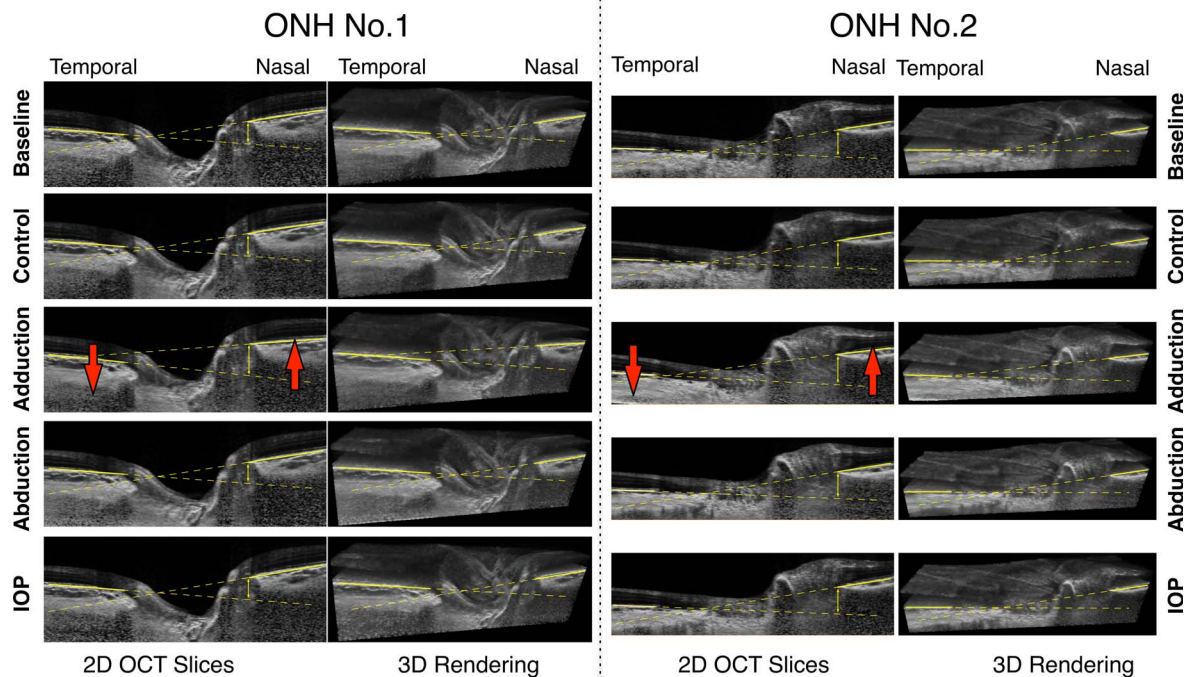
FIGURE 2. Colocalized B-scans of the ONH (horizontal cross-section) and 3D-rendered OCT volumes (cropped) for one eye of two subjects in the baseline position, for the repeated scan (control), in adduction, in abduction and following IOP elevation. Bruch's membrane is highlighted with *yellow lines*. The *red arrows* indicate shearing of the ONH tissues in adduction (with a change in Bruch's membrane configuration). To ease visualization of the resulting ONH deformations, the same images were looped back-and-forth between the baseline and each loading scenario as shown in Supplementary Videos S1 and S2.

reconstructed LC geometry (baseline). From such displacement fields, strains can be derived.

Note that for 3D structures such as the ONH, local deformations can be difficult to interpret, as tension, compression, and shear can coexist at a single tissue point. These complex deformations can be measured by various components of strain—the gold standard measure of deformation. Among all kinds of strains, effective strain is a single index that conveniently summarizes the 3D state of strain at a local tissue location and that takes into account both compressive and tensile effects (see Supplementary Text Box for a more detailed description). Therefore, in this study, we derived local effective strains for each LC (from the displacement fields[9,10]) and reported the mean effective strain of each LC for all eyes.

To report LC displacements, we first divided each LC into nasal and temporal halves using a sagittal plane that passed through the center of the best-fitted ellipse to Bruch's membrane opening (BMO; manually delineated for all baseline volumes). Mean displacements in the anteroposterior direction were calculated for each half (temporal and nasal) of each LC. Relative displacements were reported for all loading scenarios, by subtracting the mean displacements of the nasal LC from that of temporal LC. Note that a large relative displacement would indicate shearing of the LC in the anteroposterior direction (i.e., in the transverse B-scan plane).

Statistical Analysis

Means and standard deviations of effective LC strains for each loading scenario (i.e., control, adduction, abduction, IOP increase) were calculated.

We used Wilcoxon signed rank tests to test whether LC strains induced by adduction, abduction, or IOP were significantly higher than the control deformations (between the baseline and repeated scans). The same test was used to compare and rank strain levels across all three loading scenarios (adduction, abduction, and IOP).

In our previous report, we speculated that eye movements might contribute to the formation of PPA through the pulling action of the ON sheaths.[16] Therefore, in this study, we additionally compared LC strains (induced by adduction, abduction and IOP) in eyes with and without PPA using a Mann-Whitney U test.

All analyses were performed using a computing environment (MATLAB, Version 2015a; MathWorks, Inc., Natick, MA, USA). A value of $P < 0.05$ was considered statistically significant.

RESULTS

ONH Deformations—Qualitative Description

Colocalized B-scans of the ONH (horizontal cross-section) and 3D-rendered OCT volumes (cropped) are shown in Figure 2 for one eye of two subjects in the baseline position, for the repeated scan (control), in adduction, in abduction, and following IOP elevation. In Figure 2, Bruch's membrane is highlighted with yellow lines. To ease visualization of the resulting ONH deformations, the same images were looped back-and-forth between the baseline and each loading scenario as shown in Supplementary Videos S1 and S2.

ONH Deformations—Control Conditions: Unaltered IOP and Gaze Position. Slight ONH deformations were observed between the baseline and the repeated (control) OCT volumes (Supplementary Videos S1, S2), and this was consistent for all eyes. There were no noticeable changes in Bruch's membrane configuration (yellow lines, Fig. 2).

ONH Deformations Following Changes in Gaze Position. In adduction, we observed a clear change in Bruch's membrane configuration compared with baseline (Fig. 2).
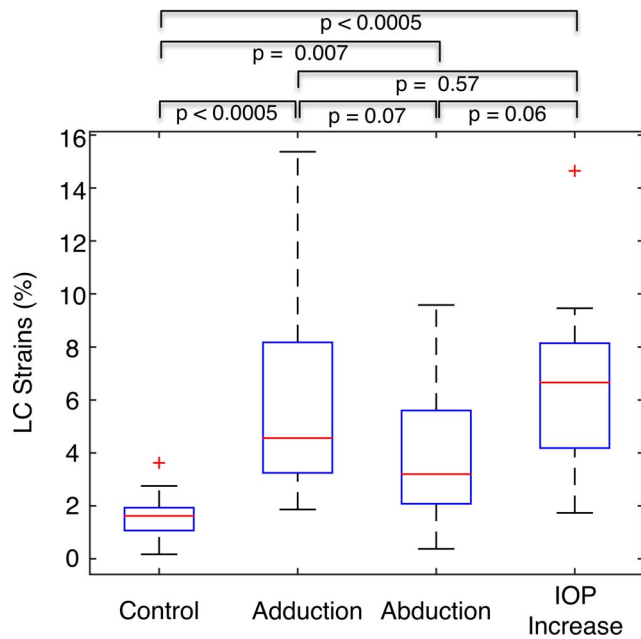
FIGURE 3. Box plots of mean LC effective strains for all 16 eyes and for all loading scenarios (control, adduction, abduction, and IOP increase). The strains induced by abduction (20°); adduction (20°); and IOP elevation (21.13 ± 7.61 mm Hg) were all statistically higher than the control strains.

Specifically, we observed a shearing deformation of the ONH tissues in the transverse plane (Supplementary Videos S1, S2; red arrows in Fig. 2) with temporal pulling and nasal compression possibly due to the action of the ON sheaths. These shearing deformations were also evident through 3D volume rendering visualization. Deformations of ONH in abduction were present but less striking. This behavior was highly consistent across all eyes.

ONH Deformations Following Acute IOP Elevation. Elevation of IOP (1st subject, 16–45 mm Hg; 2nd subject, 16–38 mm Hg) resulted in compression of the prelaminar tissues, scleral canal opening, and changes in LC curvature (Supplementary Videos, S1, S2). Bruch's membrane configuration was only slightly affected (Fig. 2). This behavior was highly consistent across all eyes.

ONH Deformations—Quantitative Descriptions

LC Strains—Control Conditions: Unaltered IOP and Gaze Position. For the controls (no alterations in IOP and in gaze position), LC effective strains for all 16 eyes were relatively small ($1.62\% \pm 0.81\%$).

LC Strains Following Changes in Gaze Position. In all 16 eyes, LC effective strains induced by adduction (20°) and abduction (20°) were $5.83\% \pm 3.78\%$ and $3.93\% \pm 2.57\%$, respectively, and both significantly higher than the control strains ($P < 0.0005$ for adduction, and $P = 0.007$ for abduction; Fig. 3). Strains of LC in adduction were on average higher than those in abduction, but the difference was only statistically significant at the 0.1 level ($P = 0.07$).

LC Strains Following Acute IOP Elevation. Strains of LC induced by IOP elevations (on average 21.13 ± 7.61 mm Hg) were $6.41\% \pm 3.21\%$ and significantly higher than the control strains ($P < 0.0005$). However, LC strains induced by IOP were not significantly different from those measured in adduction ($P = 0.57$) and were only significantly different from those measured in abduction at the 0.1 level ($P = 0.06$). Note that on average, IOP-induced LC strains were the largest, followed by those induced by adduction, then by those induced by abduction. However, it was possible for some individual eyes to exhibit the largest strains in adduction (see LC strain maps for two subjects and for all loading scenarios in Fig. 4; for 1 subject, the IOP-induced strains are the highest, while for the other the strains in adduction are the highest).

Relative LC Displacements Between Nasal and Temporal Sectors. Relative LC displacements (indicative of LC shearing in the transverse plane) are summarized in Figure 5. They were elevated in adduction (8.26 ± 14.93 μm) and were near zero in the controls (-0.13 ± 3.88 μm), in abduction (-0.90 ± 2.49 μm) and following IOP elevation (0.43 ± 2.58 μm). These results were consistent with our qualitative observations in Figure 2 and Supplementary Videos S1 and S2, in which shearing deformations in the transverse plane were only apparent for adduction.

LC Strains Following Eye Movements—Links With Peripapillary Atrophy. We found that LC effective strains in adduction and in abduction in the PPA group were larger than those in the non-PPA group as shown in Table 2. However, the relationship was not statistically significant ($P = 0.145$ for adduction and $P = 0.115$ for abduction).

DISCUSSION

Our study used an OCT-based 3D tracking technology to quantitatively map in vivo LC deformations induced by eye movements and following acute IOP elevations. We demonstrated that LC strains in adduction were large and comparable to those following a substantial IOP increase to 30 to 40 mm Hg, which is in agreement with our previous finite element predictions.[7]
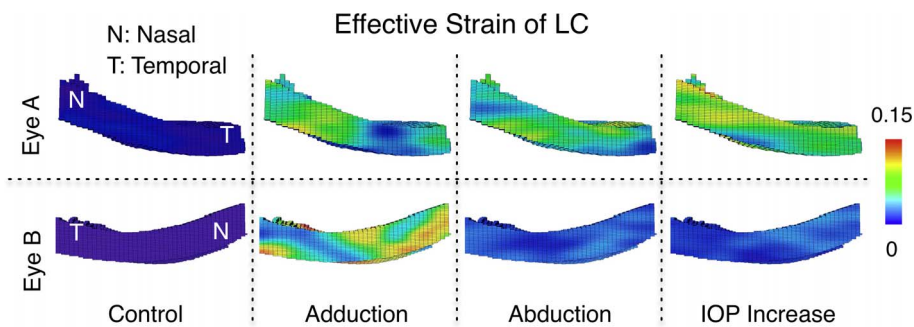
FIGURE 4. Color maps (cropped) of LC effective strains for one eye of two subjects for all loading scenarios (control, adduction, abduction, and IOP increase). For eye (**A**), IOP-induced strains were larger (on average) than those induced by adduction and abduction. For eye (**B**), adduction yielded the highest LC strains.
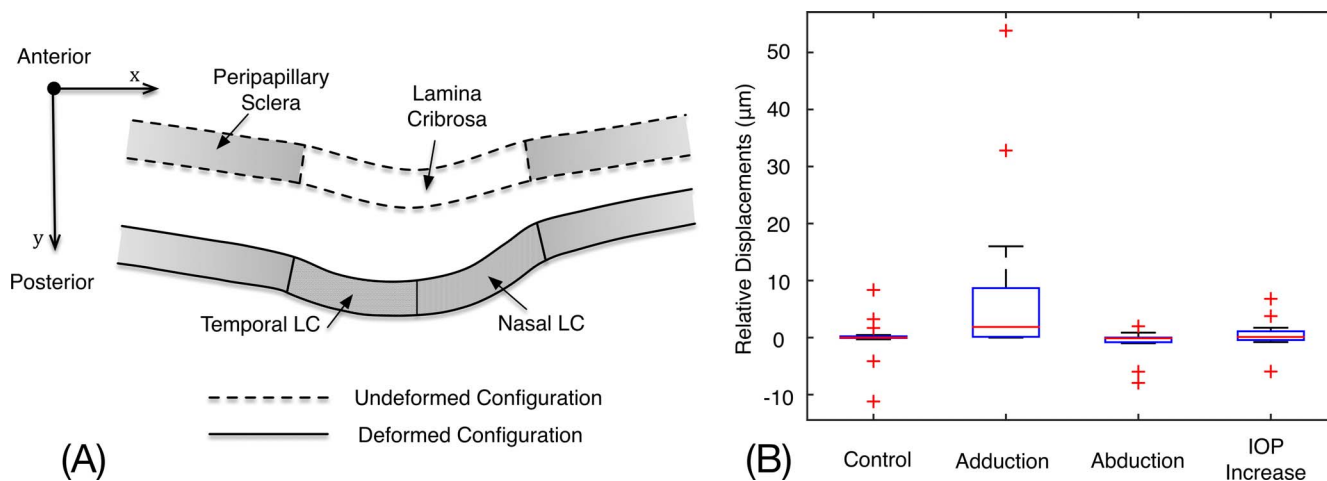
FIGURE 5. (A) Schematic of an ONH in its nondeformed and deformed configurations. The lamina cribrosa was divided into nasal and temporal halves to compute relative displacements. These latter were calculated by subtracting the mean displacement of the nasal LC in the anteroposterior direction (y direction in [A]) from that of the temporal LC. (B) Box plot of relative displacements for all loading scenarios (control, adduction, abduction, IOP elevation).

Deformations of LC induced by eye movements were visible from direct observations of OCT images (Supplementary Videos S1, S2; Fig. 2). Furthermore, 3D tracking showed that gaze-induced LC strains were significantly higher than the control strains but not statistically different from those induced by an IOP elevation to approximately 35 to 40 mm Hg (Fig. 3), indicating that gaze-induced LC deformations were realistic. We speculate that large ONH deformations following eye movements are the results of the pulling action of the ON sheaths.

Strains of LC induced by adduction were on average higher than those induced by abduction, which is also consistent with our previous finite element predictions.[7] This may be explained by the way the ON deforms and alters its length following either adduction or abduction. For instance, the change in distance between the ONH and the orbital apex (where the ON enters the optic canal) during eye movements can be evaluated through a simple geometrical analysis (see MRI image of the orbit in Fig. 6). From Figure 6, we can observe that the change in ONH/orbital apex distance following adduction ($c_2 - b$) is larger than that following abduction ($c_2 - b$), simply because the orbital apex is located nasally to the ONH axis (axis that passes through the eye center and the ONH center). For the healthy eye in Figure 6, the ONH/orbital canal distance would increase by 7.4% for 20° adduction, but only by 0.8% for 20° abduction. As shown in Supplementary Table S1, this effect would be exaggerated for larger rotations angles and is highly influenced by the location of the orbital apex relative to the ONH in primary gaze position. Although the ONH/orbital canal distance does not directly reflect the ON length, its change with eye movements will likely be representative of the amount of ON stretching since the ON is fixed at the optic canal by fibrous adhesions.[17] For a small rotation in abduction, the ON could maintain its curved shape because of the small expected changes in ONH/orbital apex distance. However, in adduction, the ON may be forced to become taut to accommodate for a longer ONH/orbital apex distance. This geometrical analysis is consistent with previous observations of ON status during eye movements using MRI,[8] and could explain why ONH deformations are higher in adduction.

In the geometric analysis above, we made several assumptions that need further clarification. First, we assumed that the ON was fixed at the optic canal. Hayreh[17,18] reported that the dura in the optic canal region is firmly bounded to the
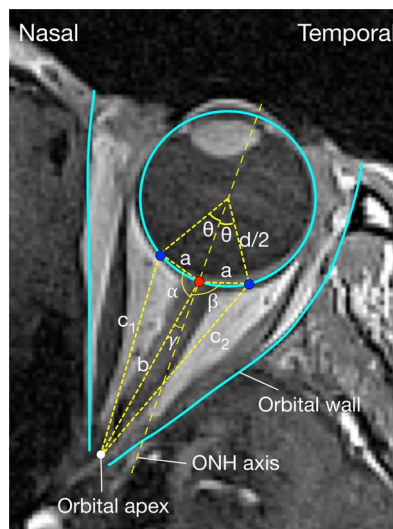
FIGURE 6. Changes of distances between orbital apex and ONH during abduction and adduction. Optic nerve head travels the same distance (from *red* to *blue point*) for the same magnitude of abduction and adduction. However, distance change for adduction is larger than that of abduction simply because the orbital apex (where the optic nerve enters the optic canal) is located nasally to the ONH axis as illustrated. The differences of c_1 and c_2 at various eye rotation magnitudes and orbital structures could be found in Supplementary Table S1. **(b)** Original distance; c_1, distance after abduction of θ; c_2, distance after adduction of θ; d, diameter of the eye globe. MRI image was taken from a 57-year old healthy female and used to illustrate locations of different tissues in the orbit.

TABLE 2. LC Strains of PPA and Non-PPA Group

Loading Scenarios	PPA, $n = 11$	Non-PPA, $n = 5$	P Value
Adduction, 20°	6.66% ± 4.11%	4.01% ± 2.33%	0.145
Abduction, 20°	4.53% ± 2.83%	2.61% ± 1.25%	0.115
IOP increase (21.13 ± 7.61), mm Hg	5.81% ± 2.07%	7.71% ± 4.99%	0.441

adjoining bone, and that the ON is connected to the dura by thick collagenous fibrous bands. These connections are thought to firmly hold the ON in position in the optic canal region. However, it is still plausible that such connections would be "weak" in some individuals. If it was the case, the pulling action of the ON onto the ONH during eye movements would be reduced, and so would the resulting ONH strains. Interestingly, when allowing the ON to slide over the optic canal in our finite element simulations, we found that LC strains were indeed reduced, but by a small amount (7% reduction) and such strains remained relatively large.[7] Second, we assumed the center of the eye hardly displaced during eye movements. However, it has been reported that the eye globe could be retracted posteriorly in highly myopic eyes with staphyloma during eye movements.[8] Although globe retraction could most likely be caused by the pulling action of the ON, it is still plausible that, in some eyes, the entire globe could move actively in the posterior direction to release the stress exerted on the ON and the ONH. Nevertheless, even if globe retraction would reduce ON/ONH stresses, the eye would most likely go through a temporary state of high ONH stress due to a mismatch in mechanical properties between the ON and ONH tissues. Further studies are needed to fully assess the link between eye retraction during eye movements and ON/ONH stretching. Third, it is possible that the ON (or the dura-sclera junction) exhibits a state of "slack" in the primary gaze position that could considerably reduce the resulting ONH strains during eye movements. However, our previous finite element simulations still demonstrated large ONH strains during eye movements even though the "slack" status of the ON was taken into account.[7] Specifically, at the macroscopic level, the slack of the optic nerve was considered by taking into account the original curvature of the ON. At the microscopic level, the slack of collagen fibers was reflected in the dura/pia nonlinear material properties (measured in ex vivo porcine eyes and used in the models to mimic the uncrimping of the collagen fibers with stretch). Because, we estimated the "slack" status from ex vivo porcine eyes, it may not be representative of the in vivo status and further in vivo studies are required. However, by taking all our works together (finite element, OCT, and geometrical analyses), strong evidence suggests that large ONH strains during eye movements are most likely the result of the pulling action of the ON.

Previous studies have investigated ONH deformations induced by IOP[10,19] or by CSFP.[20] To the best of our knowledge, no studies have yet quantified ONH strains following eye movements. In our study, the eye rotation amplitude was 20°. Given that human eyes can rotate up to a maximum of approximately ±50° in daily activities,[21] even larger ONH deformations should be expected. It is notable that IOP-induced ONH deformations are chronic and those induced by eye movements are transient. However, the human ocular globes perform constant exploratory diurnal saccades and pursuit movements, as well as during sleep (rapid eye movements[22]). We speculate that these transient deformations may have a long-term impact on the ONH by constantly deforming the ONH tissues.

Although, on average, IOP-induced LC strains were the largest, followed by those induced by adduction, this was not the case for all individual eyes. Some eyes were more susceptible to gaze changes while others were more sensitive to IOP elevation as shown in Figure 4. A possible explanation for these differences is that IOP-induced ONH deformations are likely governed by the morphologic and mechanical characteristics of the ONH tissues,[23] while aside from ONH properties, gaze-induced ONH deformations may also be affected by the properties of the ON. For instance, it is highly plausible that the amount of ON "slack" in primary gaze position could vary widely across individuals, and a smaller amount of slack in some individuals may result in larger ONH deformations during eye movements due to a rapid straightening effect of the ON. In addition, our previous finite element study suggested that gaze-induced ONH deformations were highly influenced by the stiffness of the sclera and by that of the ON dura sheath.[7] Specifically, we found that a stiffer dura sheath will tend to restrict eye movements by exerting a larger pulling force on the ONH. It is also plausible that dural stiffness would vary widely across individuals, and further studies on the biomechanics of the dura are warranted.[7,24]

If the pulling action of the ON can deform the ONH, it might be large enough to restrict eye movements. Previous studies on ocular motility mainly focused on the forces generated by extraocular muscles.[25] Our study suggests that the passive force generated by the ON may be another significant load acting on the mobility of the eye globes. Although at present, the magnitude of this force is unknown, one study has demonstrated that it was large enough to significantly retract the eye globe within its orbit in highly myopic eyes with staphyloma.[8] An improved knowledge of the force exerted by the ON on the eye globe may improve our understanding of multiple ophthalmic pathologies such as glaucoma and myopia.

We found that LC strains induced by eye movements in the PPA group were larger than those in the non-PPA group. However, this result did not reach statistical significance ($P = 0.145$ for adduction and $P = 0.115$ for abduction), potentially because of the small sample size ($n = 11$ and $n = 5$). In our previous finite element study,[16] we observed large stress concentrations near the scleral canal following eye movements, which may cause shearing between the RPE layer and Bruch's membrane.[11] These gaze-induced stresses could potentially lead to the formation of peripapillary beta and gamma zones, but more evidence is required.

Large LC deformations during eye movements in some eyes may shed light on the mechanisms involved in normal-tension glaucoma (NTG). Previous biomechanical explanations of normal tension glaucoma assumed that the LC of NTG eyes might have weaker than normal LCs (i.e., lower structural stiffness; see definition in Supplementary Text Box) that are more susceptible to IOP elevations,[26] or instead, lower CSFP.[27] Our study proposes an alternative pathway for axonal damage (through eye movements) in eyes in which IOP is not elevated. Further studies of eye movements in NTG subjects should be performed.

Eye movements may also have implications for the development of myopia. If the pulling action of the ON is larger than normal in certain eyes (e.g., because of a short ON or stiff dural sheath), repeated stretching of the sclera during eye movements may contribute in part to axial elongation (through tissue remodeling) in myopia. Furthermore, the association between myopia and glaucoma may be linked through eye movement. We know that high myopia is a risk factor for glaucoma and there is a strong correlation between these two pathologies.[28] The eye presents some similar structural changes in high myopia and glaucoma such as peripapillary atrophy.[29] Therefore, it is possible that, similar structural changes in glaucoma and high myopia might share the same cause—abnormal ON stretching of the ONH during eye movement.

In this study, several limitations warrant further discussion. First, our study was limited to a small group of normal subjects. Although LC strains induced by eye movements were large in all subjects, studying a larger cohort (including glaucoma subjects) would be beneficial.

Second, the eye rotation angles were fixed at 20° for both abduction and adduction. Since human eyes can rotate up to a maximum of approximately ±50° in daily activities, larger ONH strains could be expected.[21] However, it is also possible that there exists a nonlinear relationship between the magnitude of eye rotation and the resulting ONH deformations. In the current study, the ON deformations were not studied during "natural" eye movements (i.e., saccades) and therefore, the type of tensions may not correspond entirely to real-life situations. Future studies are required to further explore the dynamics of eye movements (rapid versus slow) as well as their amplitude, in particular in extreme gaze.

Third, only the OCT-visible portions of the LC were segmented and processed for strain mapping. Therefore, our strain averages may not be representative of the posterior part of the LC.

Fourth, the effective strains in the control cases were found to be nonzero and averaged 1.62% across all 16 eyes. These strains could arise from: (1) slight IOP fluctuation across scans (e.g., from the ocular pulse)[30]; (2) retinal vein pulsation[31]; (3) registration errors of the OCT device; (4) speckle noise; and/or (5) pre- and postprocessing errors. However, it is important to emphasize that LC strains in abduction, in adduction and following IOP elevations were significantly higher than the control strains indicating that ONH deformations in all three scenarios were indeed realistic.

In conclusion, our study measured LC strains induced by eye movements in vivo for the first time. Our results confirmed large optic nerve head strains during eye movements, which is consistent with our previous estimations using finite element analysis. Further studies are needed to explore a possible link between ONH strains induced by eye movements and axonal loss in glaucoma and other pathologies.

References

1. Sommer A, Tielsch JM, Katz J, et al. Relationship between intraocular pressure and primary open angle glaucoma among white and black Americans. The Baltimore Eye Survey. *Arch Ophthalmol*. 1991;109:1090–1095.

2. Leske MC, Wu SY, Hennis A, et al. Risk factors for incident open-angle glaucoma: the Barbados Eye Studies. *Ophthalmology*. 2008;115:85–93.

3. Leske MC. Open-angle glaucoma - an epidemiologic overview. *Ophthalmic Epidemiol*. 2007;14:166–1672.

4. Leske MC, Wu SY, Hennis A, Honkanen R, Nemesure B; BESs Study Group. Risk factors for incident open-angle glaucoma. *Ophthalmology*. 2008;115:85–93.

5. Burgoyne CF, Downs JC, Bellezza AJ, Suh JK, Hart RT. The optic nerve head as a biomechanical structure: a new paradigm for understanding the role of IOP-related stress and strain in the pathophysiology of glaucomatous optic nerve head damage. *Prog Retin Eye Res*. 2005;24:39–73.

6. Kupersmith MJ, Sibony P, Mandel G, Durbin M, Kardon RH. Optical coherence tomography of the swollen optic nerve head: deformation of the peripapillary retinal pigment epithelium layer in papilledema. *Invest Ophthalmol Vis Sci*. 2011;52:6558–6564.

7. Wang X, Rumpel H, Lim WEH, et al. Finite element analysis predicts large optic nerve head strains during horizontal eye movements. *Invest Ophthalmol Vis Sci*. 2016;57:2452–2462.

8. Demer JL. Optic nerve sheath as a novel mechanical load on the globe in ocular duction. *Invest Ophthalmol Vis Sci*. 2016;57:1826–1838.

9. Girard MJ, Strouthidis NG, Desjardins A, Mari JM, Ethier CR. In vivo optic nerve head biomechanics: performance testing of a three-dimensional tracking algorithm. *J R Soc Interface*. 2013;10:20130459.

10. Girard MJA, Beotra MR, Chin KS, et al. In vivo 3-dimensional strain mapping of the optic nerve head following intraocular pressure lowering by trabeculectomy. *Ophthalmology*. 2016;123:1190–1200.

11. Dai Y, Jonas JB, Huang H, Wang M, Sun X. Microstructure of parapapillary atrophy: beta zone and gamma zone. *Invest Ophthalmol Vis Sci*. 2013;54:2013–2018.

12. Tun TA, Thakku SG, Png O, et al. Shape changes of the anterior lamina cribrosa in normal, ocular hypertensive, and glaucoma eyes following acute intraocular pressure elevation. *Invest Ophthalmol Vis Sci*. 2016;57:4869–4877.

13. Girard MJ, Strouthidis NG, Ethier CR, Mari JM. Shadow removal and contrast enhancement in optical coherence tomography images of the human optic nerve head. *Invest Ophthalmol Vis Sci*. 2011;52:7738–7748.

14. Girard MJ, Tun TA, Husain R, et al. Lamina cribrosa visibility using optical coherence tomography: comparison of devices and effects of image enhancement techniques. *Invest Ophthalmol Vis Sci*. 2015;56:865–874.

15. Wells WM III, Viola P, Atsumi H, Nakajima S, Kikinis R. Multimodal volume registration by maximization of mutual information. *Med Image Anal*. 1996;1:35–51.

16. Wang X, Rumpel H, Lim WEH, et al. Author response: peripapillary suprachoroidal cavitation parapapillary gamma zone and optic disc rotation due to the biomechanics of the optic nerve dura mater. *Invest Ophthalmol Vis Sci*. 2016;57:4374–4375.

17. Hayreh SS. Structure of the Optic Nerve. Ischemic Optic Neuropathies. Berlin: Springer-Verlag; 2011:7–34.

18. Hayreh SS. The sheath of the optic-nerve. *Ophthalmologica*. 1984;189:54–63.

19. Jiang R, Xu L, Liu X, Chen JD, Jonas JB, Wang YX. Optic nerve head changes after short-term intraocular pressure elevation in acute primary angle-closure suspects. *Ophthalmology*. 2015;122:730–737.

20. Sibony P, Kupersmith MJ, Honkanen R, Rohlf FJ, Torab-Parhiz A. Effects of lowering cerebrospinal fluid pressure on the shape of the peripapillary retina in intracranial hypertension. *Invest Ophthalmol Vis Sci*. 2014;55:8223–8231.

21. Land MF. Eye movements and the control of actions in everyday life. *Prog Retin Eye Res*. 2006;25:296–324.

22. Hobson JA. REM sleep and dreaming: towards a theory of protoconsciousness. *Nat Rev Neurosci*. 2009;10:803–813.

23. Sigal IA, Flanagan JG, Ethier CR. Factors influencing optic nerve head biomechanics. *Invest Ophthalmol Vis Sci*. 2005;46:4189–4199.

24. Raykin J, Forte TE, Wang R, et al. Characterization of the mechanical behavior of the optic nerve sheath and its role in spaceflight-induced ophthalmic changes. *Biomech Model Mechanobiol*. 2016:1–11.

25. Schutte S, van den Bedem SP, van Keulen F, Simonsz HJ. A finite-element analysis model of orbital biomechanics. *Vision Res*. 2006;46:1724–1731.

26. Park H-YL, Jeon SH, Park CK. Enhanced depth imaging detects lamina cribrosa thickness differences in normal tension

glaucoma and primary open-angle glaucoma. *Ophthalmology.* 2012;119:10–20.

27. Berdahl JP, Fautsch MP, Stinnett SS, Allingham RR. Intracranial pressure in primary open angle glaucoma, normal tension glaucoma, and ocular hypertension: a case–control study. *Invest Ophthalmol Vis Sci.* 2008;49:5412–5418.

28. Xu L, Wang Y, Wang S, Wang Y, Jonas JB. High myopia and glaucoma susceptibility the Beijing Eye Study. *Ophthalmology.* 2007;114:216–220.

29. Vianna JR, Malik R, Danthurebandara VM, et al. Beta and gamma peripapillary atrophy in myopic eyes with and without glaucoma beta- and gamma-PPA in myopic glaucoma diagnosis. *Invest Ophthalmol Vis Sci.* 2016;57:3103–3111.

30. Downs JC, Burgoyne CF, Seigfreid WP, et al. 24-hour IOP telemetry in the nonhuman primate: implant system performance and initial characterization of IOP at multiple time-scales. *Invest Ophthalmol Vis Sci.* 2011;52:7365–7375.

31. Morgan WH, Lind CRP, Kain S, et al. Retinal vein pulsation is in phase with intracranial pressure and not intraocular pressure vein pulsation phase relations. *Invest Ophthalmol Vis Sci.* 2012;53:4676–4681.

Investigative Ophthalmology & Visual Science